

# Colorimetric and spectroradiometric characteristics of narrow-field-of-view clear skylight in Granada, Spain

Javier Hernández-Andrés and Javier Romero

*Departamento de Óptica, Facultad de Ciencias, Universidad de Granada, Granada 18071, Spain*

Raymond L. Lee, Jr.

*Mathematics and Science Division, United States Naval Academy, Annapolis, Maryland 21402*

Received May 22, 2000; accepted August 21, 2000; revised manuscript received August 25, 2000

As part of our ongoing research into the clear daytime sky's visible structure, we analyze over 1500 skylight spectra measured during a seven-month period in Granada, Spain. We use spectral radiances measured within 3° fields of view (FOV's) to define colorimetric characteristics along four sky meridians: the solar meridian and three meridians at azimuths of 45°, 90°, and 315° relative to it. The resulting clear-sky chromaticities in 44 different view directions (1) are close to but do not coincide with the CIE daylight locus, (2) form V-shaped meridional chromaticity curves along it (as expected from theory), and (3) have correlated color temperatures (CCT's) ranging from 3800 K to  $\infty$  K. We also routinely observe that sky color and luminance are asymmetric about the solar meridian, usually perceptibly so. A principal-components analysis shows that three vectors are required for accurate clear-sky colorimetry, whereas six are needed for spectral analyses.

© 2001 Optical Society of America

OCIS codes: 010.1290, 330.1710, 330.1730.

## 1. INTRODUCTION

Although many researchers have studied the angular distribution of visible-wavelength radiance across the clear daytime sky, few have analyzed its color variations. A 1985 article by Bohren and Fraser<sup>1</sup> corrected some common misconceptions about the theory of sky colors (for example, Bohren and Fraser note that uncritical use of Rayleigh's scattering theory leads to the false conundrum that the clear daytime sky should be violet), but little experimental work has followed their lead. In fact, nearly all subsequent research has been devoted to developing empirical and theoretical models of clear-sky radiance and luminance across the sky dome.<sup>2-6</sup> By contrast, relatively few studies have dealt with the angular distribution of clear-sky spectra and chromaticities.<sup>7-10</sup>

Yet skylight's spectral and color distributions are often as important in theoretical and applied work as are its radiance patterns. For example, skylight spectra can dictate the design and performance of spectrally selective solar-energy devices such as photovoltaic systems. Improving our knowledge of clear-sky spectra is valuable in many research areas, ranging from aircraft flight simulation and daylighting predictions to developing radiation models for predicting climate change and its biological effects. Here we present one contribution to the larger goal of developing a modern, truly worldwide basis for measuring and analyzing the clear sky's colors.

What is the current state of clear-sky color modeling and measurement? In 1991 Sekine modeled skylight colors, considering separately the effects of aerosol optical

depth, solar elevation, reflected surface light, and scattering angle.<sup>11</sup> Several years later, one of us used digital image analysis<sup>12</sup> to measure daytime and twilight clear-sky chromaticities along meridians near the horizon.<sup>13</sup> Among other points, this study showed that near-horizon chromaticity curves need not parallel the Planckian (or blackbody) locus. In 1999, Chain *et al.*<sup>10</sup> found an empirical relationship between correlated color temperature (CCT) and luminance under clear skies. This development let them use the CIE method<sup>14</sup> to derive skylight spectra from luminances alone.

Skylight spectra have been measured within narrow fields of view (FOV's) in past decades,<sup>15-28</sup> but the instruments available then ruled out quick, systematic mapping of the entire sky. We now have the luxury of fast, narrow-FOV spectroradiometers that let us compile such quasi-instantaneous skylight maps. Another reason to revisit sky color is that older papers' terminology is itself confusing, sometimes not distinguishing between "daylight" and "skylight." To avoid this ambiguity, we follow convention and distinguish between (1) hemispheric *daylight* that can include direct sunlight and (2) narrow-FOV *skylight* that always excludes direct sunlight. In fact, chromaticity curves for daylight irradiances and skylight radiances usually will differ at a given place (consider, say, daylight and skylight chromaticity curves measured for one hour at fixed detector orientations). This is true because skylight, unlike daylight, is measured within small FOV's and in many different directions. Other parameters that affect sky color are the observing site's lo-

cation and altitude, the sky state, and the length of time required for each measurement. We discuss these parameters for our site in the next section.

In Sections 3 and 4 we analyze the angular and short-term temporal trends in skylight colors calculated from our measured narrow-FOV spectral radiances. We acquired these spectra during a seven-month period at one site for a wide variety of solar elevations  $h_0$  and view directions. The resulting chromaticities are considered not only *en masse*, but also as individual points that form chromaticity curves as functions of view-elevation angle  $h$  along particular sky meridians ( $h$  is positive above the astronomical horizon). In addition, we use principal value decompositions to examine the correlations among our skylight spectra. These correlations tell us how many eigenvectors are required in linear skylight models to make our color identification and recognition reliable.<sup>29,30</sup>

## 2. EXPERIMENTAL PROCEDURE

To measure spectral radiances across the sky dome, we used a LI-COR model LI-1800 spectroradiometer that we coupled via fiber-optic cable to a small refracting telescope with a  $3^\circ$  (0.00215 sr) FOV.<sup>31</sup> The LI-1800 radiometer's optical characteristics have been described in detail by other researchers.<sup>32–34</sup> In our work the LI-1800's spectral range was limited to the visible (380–780 nm), and its wavelength resolution was 5 nm. Because the LI-1800 takes 12 s to acquire a visible spectrum, practically speaking we could measure as many as 3 spectra/min. We fixed the viewing telescope to a pyrhelimeter mount that let us aim the telescope manually in the desired view direction. Uncertainties in setting  $h$  and relative azimuth  $\phi_{\text{rel}}$  were  $0.1^\circ$  and  $1^\circ$ , respectively.

Figure 1 shows the  $h$ ,  $\phi_{\text{rel}}$  at which we measured skylight spectra. We chose four meridians: the solar meridian (or the clear-sky principal plane) with  $\phi_{\text{rel}} = 0^\circ$ ,

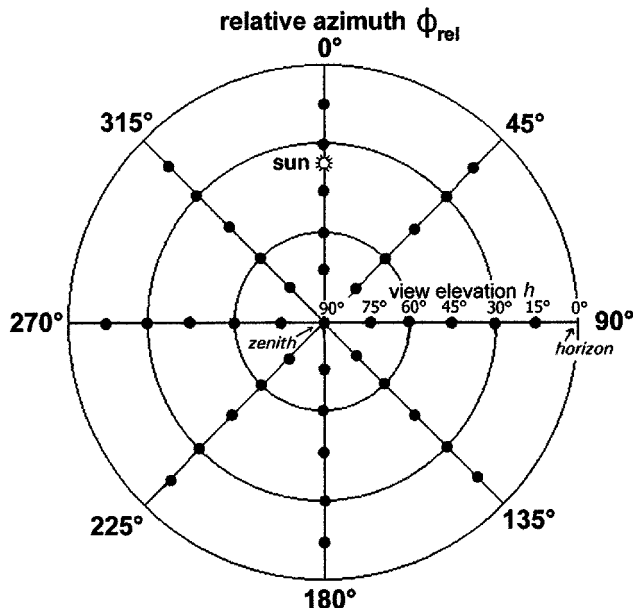


Fig. 1. Azimuths relative to the sun  $\phi_{\text{rel}}$  and view elevations  $h$  above the astronomical horizon at which we measured Granada skylight spectra.

and three meridians at  $\phi_{\text{rel}}$  of  $45^\circ$ ,  $90^\circ$ , and  $315^\circ$  angles to it. Following convention, we make  $\phi_{\text{rel}}$  increase clockwise from the sun's azimuth (i.e.,  $\phi_{\text{rel}}$  increases in the same sense as compass direction). To simplify our notation, we denote view elevations beyond the zenith as having the original  $\phi_{\text{rel}}$  and  $h > 90^\circ$ . Thus in our notation  $\phi_{\text{rel}} = 45^\circ$ ,  $h = 105^\circ$  is equivalent to  $\phi_{\text{rel}} = 225^\circ$ ,  $h = 75^\circ$  (see Fig. 1). Along each sky meridian, we made measurements in  $15^\circ$  steps for  $15^\circ \leq h \leq 165^\circ$ . As a result, each set of all-sky measurements consisted of 44 observations that required 20 min to complete. At the beginning and middle of each set, we calculated the sun's position and calibrated the telescope's  $\phi_{\text{rel}}$  by centering the sun in its FOV.

Our measurement site is in Granada, Spain (latitude  $37^\circ 11' \text{N}$ , longitude  $3^\circ 35' \text{W}$ , altitude 680 m), a city that has no significant sources of industrial aerosols. Our visual prerequisite for taking measurements was that the sky must appear to be cloudless. Between February and August 1998 we measured 1567 skylight spectra that met this requirement, and their associated  $h_0$  ranged from  $-0.6^\circ$  to  $62.2^\circ$ .

## 3. COLORIMETRIC CHARACTERISTICS

### A. Chromaticity Coordinates

Our spectra include view elevations and solar elevations that yield chromaticities typical of the blues observed in clear daytime skies. Thus none of our measurements reflect the far wider chromaticity gamut seen in the twilight sky,<sup>13</sup> a phenomenon that we are currently investigating.

Figure 2 shows the CIE 1931 chromaticities of all Granada clear skylight measurements overlaid with both the Planckian locus and the CIE daylight locus.<sup>35</sup> Figure 2 also includes our Granada skylight locus, which is above and nearly parallel to the CIE locus (i.e., toward the greens). A least-squares fit to our observed chromaticities gives the Granada skylight locus as

$$y = -0.24770 + 2.72203x - 2.77935x^2. \quad (1)$$

The chromaticity gamut of our experimental clear-sky measurements is broader than earlier ones,<sup>15–28</sup> despite the shorter time period of our study. None of our skylight spectra yield chromaticities below the Planckian locus, and most chromaticities ( $\sim 90\%$ ) are above the CIE locus. For CCT's  $< 7000$  K, the Granada skylight locus is closer to the greens than any comparable daylight and skylight chromaticities published thus far. Even though Granada's skylight chromaticities have a large CCT range, our locus, Eq. (1), describes them quite well. In fact, the square of the correlation coefficient for Eq. (1) is  $R^2 = 0.967$ , meaning that our chromaticities have negligible scatter in the green–pink directions. In fact, the 95% confidence interval in chromaticity distance about the locus of Eq. (1) ranges from a maximum of 0.001 for CCT  $> 4000$  K to a maximum of 0.005 for CCT  $< 4000$  K (because there are fewer measurements at these smaller CCT's).

Would our skylight chromaticities exhibit more scatter if we measure them within a much smaller FOV (say,  $0.25^\circ$ )? To answer this question, consider its corollary: Do Granada daylight chromaticities from hemispheric

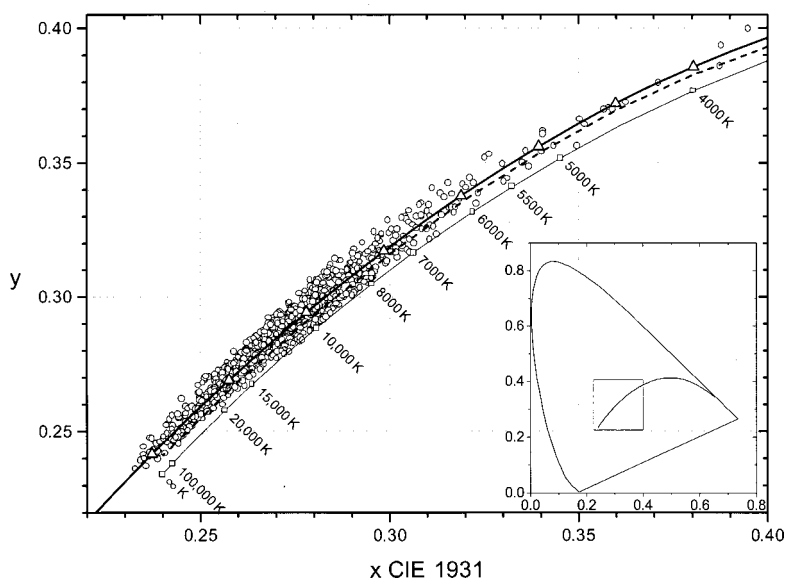


Fig. 2. CIE 1931 chromaticities of our 1567 Granada clear skylight spectra (open circles), overlaid with the CIE daylight locus (dashed curve), the Planckian locus (curve with open squares), and the Granada clear skylight locus [curve with open triangles; Eq. (1)]. The inset shows the entire CIE 1931 diagram and Planckian locus.

skylight irradiances (i.e., daylight minus direct sunlight) show significantly less scatter than our 3°-FOV skylight chromaticities? When we compare the two kinds of clear-sky chromaticities, in fact we find no statistically significant decrease in the scatter of daylight chromaticities, even though they are derived from a cosine-corrected hemispheric FOV. This suggests that if we measured skylight spectra by using a much smaller FOV, the scatter in our results would not change in any meaningful way. Of course, this is very different from our statement above that daylight and skylight chromaticity curves generally will differ at a given place.

### B. Correlated Color Temperatures

Numerous researchers have shown that CCT provides accurate estimates of daylight's visible-wavelength power spectra,<sup>15–28</sup> and this makes CCT a useful shorthand for specifying the colorimetric and spectral characteristics of daylight. The CIE exploits this relationship by using

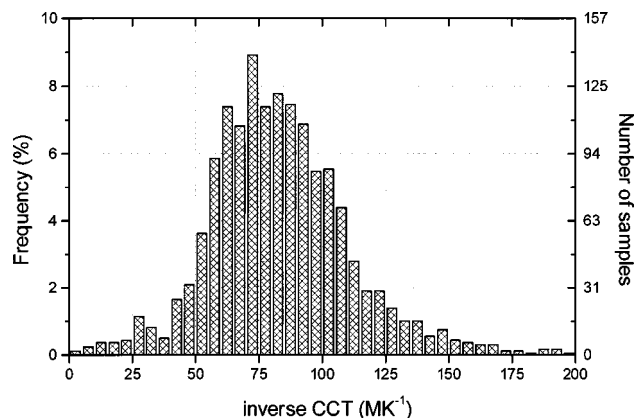


Fig. 3. Histogram of inverse CCT (in reciprocal megaKelvins) corresponding to our Granada skylight chromaticities. Some low-frequency outliers are excluded.

CCT's from 4000 K to 25,000 K to estimate the relative spectral irradiances  $E_\lambda$  of typical daylight phases at the Earth's surface.<sup>36</sup>

Our spectroradiometer's software is not designed to calculate CCT's  $> 10^5$  K, chiefly because it relies on older techniques for approximating CCT. This design limitation sometimes posed problems for us in measuring skylight CCT's, since these sometimes exceed  $10^5$  K. In a recent paper we described a simple, accurate CCT algorithm that avoids this limitation.<sup>37</sup> For the Granada skylight chromaticities, our algorithm calculated CCT's ranging from 3804 K to more than  $10^5$  K (six chromaticities had CCT's  $> 10^5$  K). Among our 1567 skylight chromaticities, only two were too far from the Planckian locus to yield spectrally meaningful CCT's.

When analyzing daylight and skylight, often it is more convenient to use inverse CCT rather than CCT itself. The unit of inverse CCT is the reciprocal megaKelvin ( $10^6/\text{CCT}$ ), denoted by the symbol  $\text{MK}^{-1}$  (historically known as the mired).<sup>38</sup> Reciprocal megaKelvins produce a uniform scale that better describes human color sensitivity than does CCT proper. On this inverse scale, the CCT range of our Granada clear-skylight data is 1.7–263.8  $\text{MK}^{-1}$ .

When this data is plotted on a histogram (Fig. 3), the most frequent inverse CCT interval is 70–75  $\text{MK}^{-1}$ . Figure 3 can be compared only imperfectly with earlier work, primarily because authors present their results in widely differing ways and because their analyses sometimes do not distinguish between skylight and daylight.<sup>15–28</sup> That caveat aside, however, Fig. 3 does differ substantially from its skylight-only predecessors.<sup>15,20,21,25</sup> Perhaps the most significant departure in Fig. 3 is its near-normal distribution of inverse CCT, a pattern observed only once before.<sup>25</sup>

### C. Meridional Chromaticity Curves

Figures 4–7 show the CIE 1931 chromaticities that we measured at different  $h$  along the solar meridian and the

meridian perpendicular to it ( $\phi_{rel} = 0^\circ, 90^\circ$ , respectively) at four different solar elevations ( $h_0 \sim 60^\circ, 20^\circ, 10^\circ, 1^\circ$ ) on three different days. Because topography did not block our view of the sky at  $h = 10^\circ$  and  $h = 5^\circ$  on two days, we also include those skylight chromaticities in Figs. 5 and 7. To aid comparisons among Figs. 4–7, we include the entire 1931 CIE diagram as an inset in each. Within each inset, we draw a small box to show the region plotted in the figure. The chromaticity curves in Figs. 4–7 are typical of those measured on many other days.

Not surprisingly, as  $h_0$  decreases, the chromaticity gamut measured along the solar meridian increases, expanding toward the yellow-orange near the sun [see especially Fig. 7(a)]. This trend is easy to interpret physically: Slant-path optical depth increases with decreasing  $h$  and  $h_0$ , and the resulting increase in direct-beam scattering makes the solar aureole yellower at a given angular radius (or scattering angle  $\Psi$ ).

However, for scans along  $\phi_{rel} = 90^\circ$ , the Granada skylight chromaticity gamuts (1) depend very little on  $h_0$  and (2) are consistently smaller than those along the solar me-

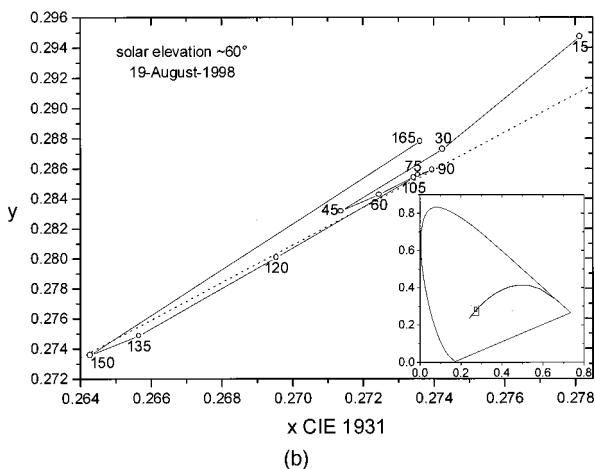
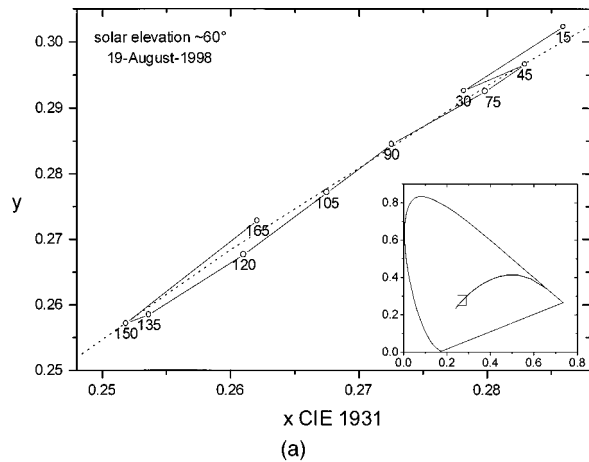


Fig. 4. (a) Chromaticity curve for Granada clear skylight along  $\phi_{rel} = 0^\circ$  (the clear-sky principal plane) when solar elevation  $h_0 = 60^\circ$  on August 19, 1998. Note that view elevations beyond the zenith are indicated by  $h > 90^\circ$ . The dotted line is the CIE daylight locus, while the inset shows the entire CIE 1931 diagram and Planckian locus. Figures 5–7 reuse Fig. 4’s notation. (b) Chromaticity curve for clear skylight along  $\phi_{rel} = 90^\circ$  when  $h_0 = 60^\circ$  (August 19, 1998).

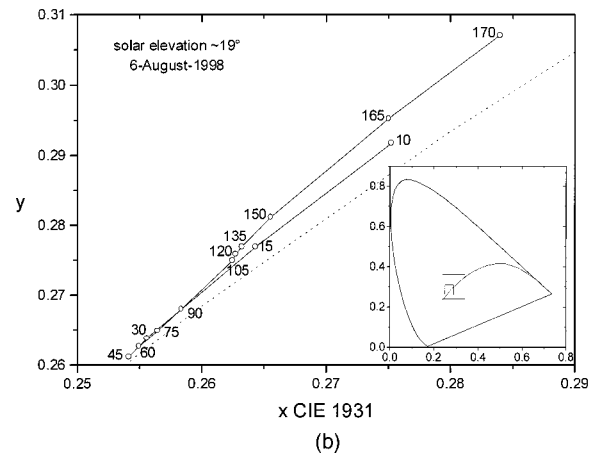
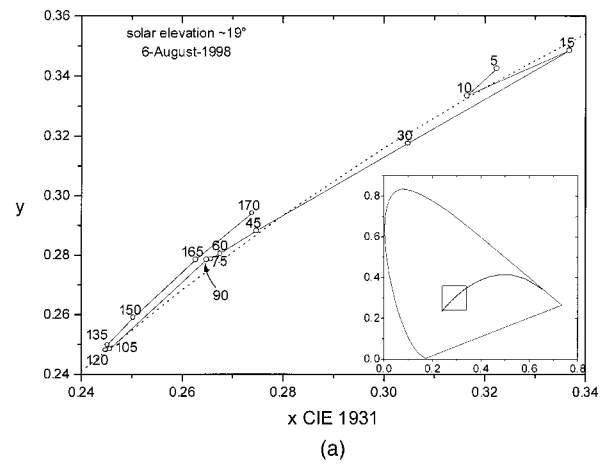


Fig. 5. (a) Chromaticity curve for clear skylight along  $\phi_{rel} = 0^\circ$  when  $h_0 = 19^\circ$  (August 6, 1998). (b) Chromaticity curve for clear skylight along  $\phi_{rel} = 90^\circ$  when  $h_0 = 19^\circ$  (August 6, 1998).

ridian. Only for  $h_0 > 30^\circ$  [see Fig. 4(b)] does the  $\phi_{rel} = 90^\circ$  gamut shrink appreciably. In fact, the chromaticities in Fig. 4(b) span a Cartesian distance of  $\sim 9$  just-noticeable differences<sup>39</sup> (JND’s) while their solar-meridian counterparts in Fig. 4(a) cover a distance more than twice as large. For  $h_0 < 30^\circ$ , chromaticity gamuts along the  $\phi_{rel} = 90^\circ$  meridian are nearly independent of sun elevation.

As Sekine shows, chromaticity curves along the solar meridian are V-shaped (possibly with a zigzag near  $h_0$  when the sun is high in the sky), and they nearly parallel the Planckian locus on its green side.<sup>11</sup> The antisolar half of these curves [i.e.,  $\phi_{rel} = 0^\circ, h > 90^\circ$ ; see Fig. 4(a)] is closer to the greens than is the solar half. The same V-shaped pattern is evident in our measured chromaticity curves for  $\phi_{rel} = 90^\circ$  [Figs. 4(b), 5(b), 6(b), and 7(b)], a relative azimuth that Sekine did not model. Our measurements also clearly show that the  $\phi_{rel} = 0^\circ$  chromaticity curves nearly coincide with the CIE locus (dashed line in Figs. 4–7), whereas their  $\phi_{rel} = 90^\circ$  counterparts lie some distance from it. This departure from the CIE locus is largest at low CCT’s ( $< 10,000$  K), where the maximum chromaticity distance just exceeds 4 JND’s.

One of the longest-standing assumptions about cloudless skies is that their chromaticity and luminance distri-

butions are symmetric about the principal plane, including along the  $\phi_{rel} = 90^\circ$  meridian. However, our measurements show something quite different in Fig. 8. To generate it, we calculate chromaticity distances between pairs of skylight colors measured at the same view elevation  $h$  along  $\phi_{rel} = 90^\circ$  (say, at  $h = 60^\circ, 120^\circ$ ). We then normalize each chromaticity distance by the appropriate JND and plot the ratios at the appropriate  $h$ . When  $h_0 = 60^\circ$ , the maximum chromaticity distance along  $\phi_{rel} = 90^\circ$  is  $\sim 2$  JND at  $h = 60^\circ$  (open squares in Fig. 8; see right ordinate). At lower  $h_0$  the maximum chromaticity distance exceeds 4 JND's at most  $h$  (open, upright triangles in Fig. 8). Thus, regardless of sun elevation, color asymmetries at the same  $h$  on either side of the principal plane *are* often perceptible. In other words, if we simultaneously compared adjacent samples of two such colors, we could distinguish between them.

Not unexpectedly, we find similar luminance asymmetries about the principal plane. In Fig. 8 the largest luminance differences ( $\sim 20\text{--}25\%$ ; see left ordinate) occur at the lowest solar elevation ( $h_0 = 0.4^\circ$ ), although these are paired with fairly small chromaticity differences. For the remaining  $h_0$ , luminance differences are  $< 8\%$ . Nonetheless, if we take a 2% luminance difference as a typical threshold for photopic vision, then nearly

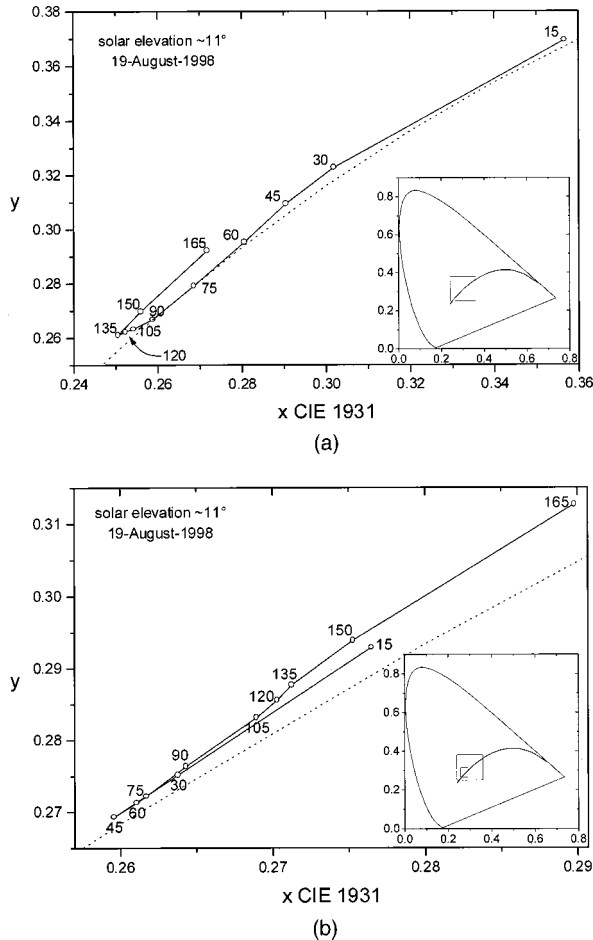


Fig. 6. (a) Chromaticity curve for clear skylight along  $\phi_{rel} = 0^\circ$  when  $h_0 = 11^\circ$  (August 19, 1998). (b) Chromaticity curve for clear skylight along  $\phi_{rel} = 90^\circ$  when  $h_0 = 11^\circ$  (August 19, 1998).

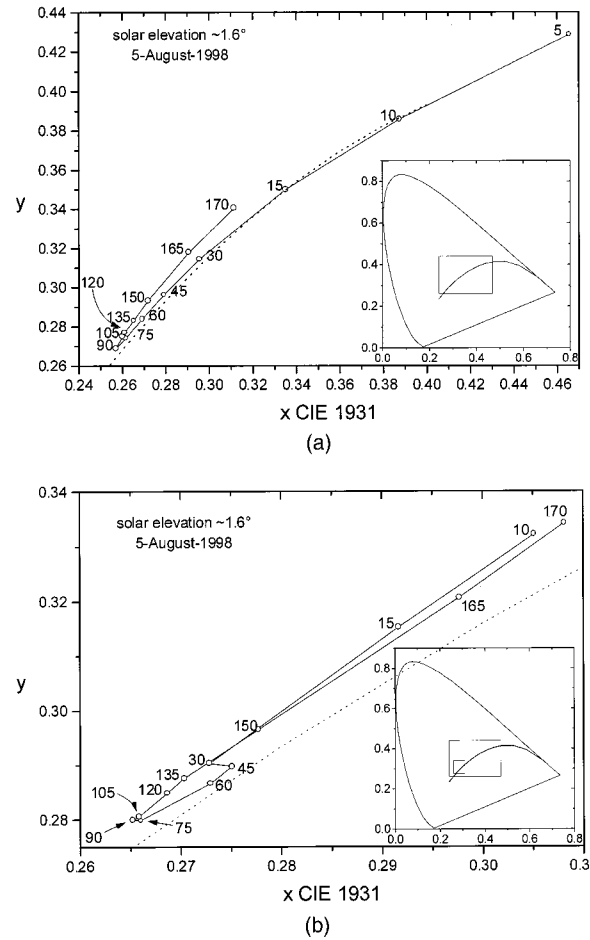


Fig. 7. (a) Chromaticity curve for clear skylight along  $\phi_{rel} = 0^\circ$  when  $h_0 = 1.6^\circ$  (August 5, 1998). (b) Chromaticity curve for clear skylight along  $\phi_{rel} = 90^\circ$  when  $h_0 = 1.6^\circ$  (August 5, 1998).

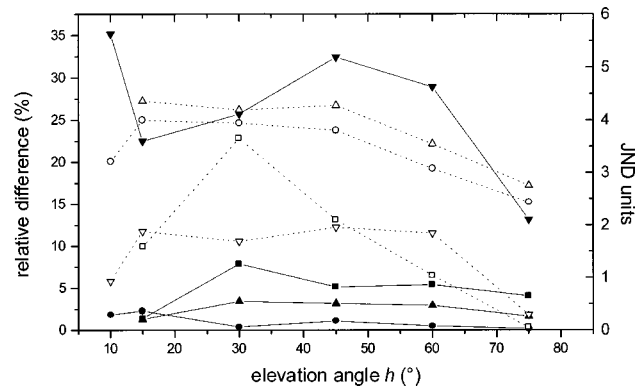


Fig. 8. Relative luminance differences (solid symbols) and chromaticity differences in JND units (open symbols) as a function of  $h$  along  $\phi_{rel} = 90^\circ$  for the four  $h_0$  shown in Figs. 4(b), 5(b), 6(b), and 7(b). Solar elevation symbols are squares for  $h_0 = 60^\circ$ , circles for  $h_0 = 18.5^\circ$ , upright triangles for  $h_0 = 10^\circ$ , and inverted triangles for  $h_0 = 0.4^\circ$ .

all of the clear sky's luminance asymmetries about the principal plane are perceptible (naturally, we rarely make the required side-by-side comparisons of skylight samples). Only for  $h_0 = 18.5^\circ$  are the Granada skylight luminance differences consistently subthreshold. Our

measurements suggest that such skylight luminance and color asymmetries are the norm, rather than the exception, in real atmospheres.

Some of this asymmetry might be ascribed to the time required to make our meridional measurements. Yet during the 4 min needed for each scan  $h_0$  changes by only  $\pm 0.5^\circ$  at high solar elevations and  $\pm 1^\circ$  at low ones. Because our uncertainty in measuring  $\phi_{rel}$  is of comparable magnitude, we believe that changes in solar position are unlikely to cause the observed asymmetries in the luminance and chromaticity of Granada's clear skies. This claim is supported by clear-sky spectra that we measured with another fast-scanning spectroradiometer. Although we acquired spectra at matching  $h$  and  $\phi_{rel}$  within a few seconds of each other, we still found perceptible differences in skylight color and luminance about the principal plane.

One plausible explanation for such asymmetries is that aerosol content varies with  $\phi_{rel}$ . In Granada this might be caused by enhanced aerosol loading from farmland west of our measurement site. The skylight asymmetries are less likely to be caused by changes in surface reflectance spectra, because these do not vary in any systematic way within 40 km of our site. Although most extant models of atmospheric scattering assume symmetry about the principal plane,<sup>2-6</sup> our results show that this assumption is only a first approximation, not an inviolable fact. Thus, to model clear-sky optics more realistically, we should add the asymmetries in color and luminance reported here to the asymmetries in polarization that we measured earlier.<sup>40</sup> Although we have not yet explicitly modeled such skylight asymmetries, recognizing their existence is a necessary first step in doing so.

We complete our colorimetric analysis in Figs. 9–12 by showing chromaticity curves along the  $\phi_{rel} = 45^\circ, 315^\circ$  meridians for  $h_0 = 58^\circ, 52^\circ, 42^\circ, 6^\circ$ . In each figure the meridional scans have similar shapes, since both are  $45^\circ$  from the principal plane. However, chromaticities can

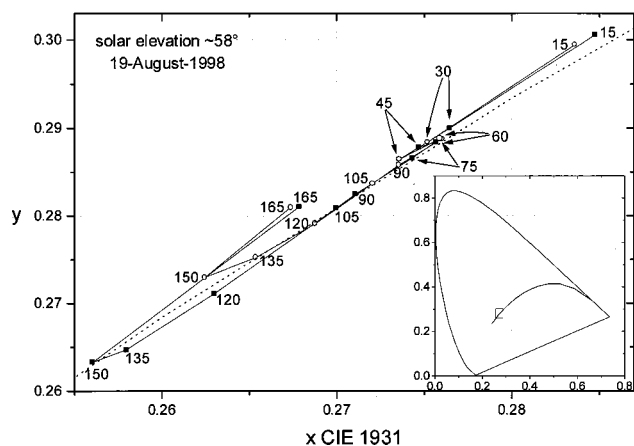


Fig. 9. Chromaticity curves for Granada clear skylight along  $\phi_{rel} = 45^\circ, 315^\circ$  when solar elevation  $h_0 = 58^\circ$  on August 19, 1998. Chromaticities along  $\phi_{rel} = 45^\circ$  are denoted with filled squares; those along  $\phi_{rel} = 315^\circ$ , with open circles. As in Figs. 4–7, view elevations beyond the zenith at each  $\phi_{rel}$  are indicated by  $h > 90^\circ$ . The dotted line is the CIE daylight locus, while the inset shows the entire CIE 1931 diagram and Planckian locus. Figures 10–12 reuse Fig. 9's notation.

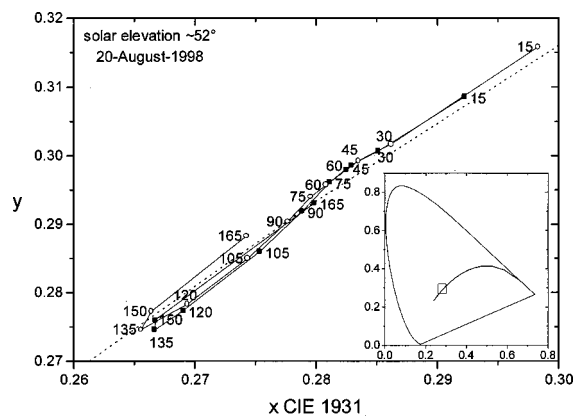


Fig. 10. Chromaticity curves for Granada clear skylight along  $\phi_{rel} = 45^\circ, 315^\circ$  when  $h_0 = 52^\circ$  (August 20, 1998).

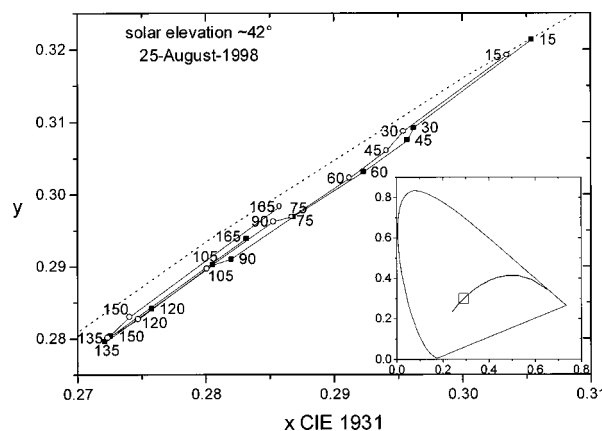


Fig. 11. Chromaticity curves for Granada clear skylight along  $\phi_{rel} = 45^\circ, 315^\circ$  when  $h_0 = 42^\circ$  (August 25, 1998).

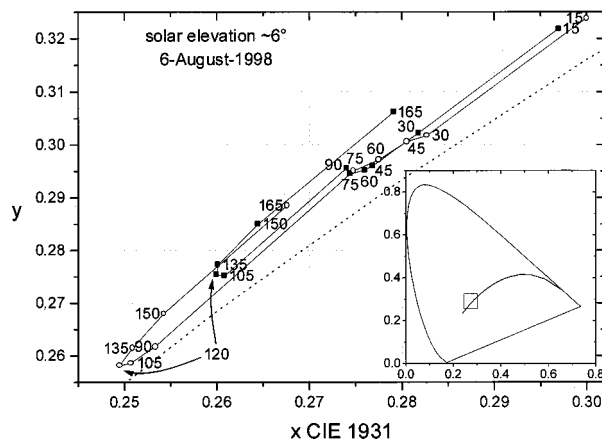


Fig. 12. Chromaticity curves for Granada clear skylight along  $\phi_{rel} = 45^\circ, 315^\circ$  when  $h_0 = 6^\circ$  (August 6, 1998).

differ markedly at the same scattering angle, such as Fig. 12's two  $h = 165^\circ$  chromaticities. At both relative azimuths, the chromaticity gamut increases with decreasing  $h_0$  as skylight is increasingly reddened by direct sunlight. Note, too, that the positions of the chromaticity curves shift from day to day, probably as a result of changes in aerosol optical depth.<sup>11</sup>

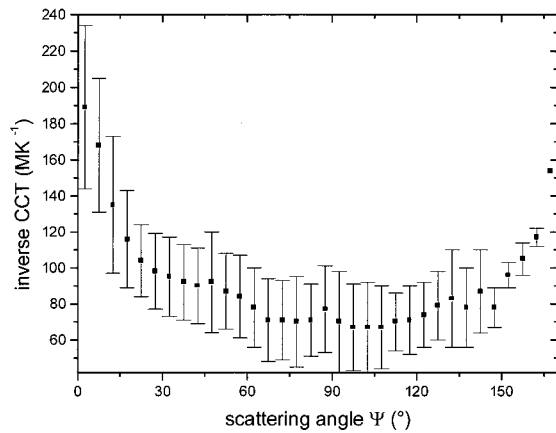


Fig. 13. Inverse CCT as a function of scattering angle  $\Psi$  for all Granada skylight chromaticities. Solid squares mark the mean inverse CCT for each  $5^\circ$ -wide bin, and error bars are 2 standard deviations wide.

#### D. Scattering Angle

Our most vivid Granada skylight had a colorimetric purity of 39.4%, while the average skylight purity was 21.6% (measured with respect to sunlight's chromaticity outside the atmosphere<sup>41</sup>). Nearly 33% of our skylight spectra had purities  $>25\%$ , and the modal dominant wavelength for all spectra was 478–479 nm. Compared with the theoretical Rayleigh purity of 41% for a single-scattering, purely molecular atmosphere, our measured purities may seem small indeed, yet they are similar to those we have measured elsewhere.<sup>13</sup> As simple theory predicts, we found that the purest blues at Granada (1) occur near  $\Psi \sim 90^\circ$  (rather than at the zenith, where optical depth is smallest) and (2) vary daily in both dominant wavelength and purity, with the large optical depths of hazy days producing the smallest maximum purities.<sup>1</sup> However, as noted below, the highest skylight purities occur not at  $\Psi = 90^\circ$ , but at somewhat larger scattering angles.

In Fig. 13 we analyze the scattering-angle dependence of Granada's skylight chromaticities in the form of inverse CCT. We first sorted our measurements into 36 scattering-angle bins between  $0^\circ$  and  $180^\circ$ , with each bin containing inverse CCT's from a  $5^\circ$  interval in  $\Psi$ . We then calculated the mean inverse CCT and its standard deviation for each bin. These standard deviations indicate the chromaticity variability caused by changes in (1)  $h_0$  and (2) slant-path molecular and aerosol optical depths. Because aerosols scatter anisotropically, Fig. 13 is not exactly symmetric about  $90^\circ$ , as it would be in a purely molecular atmosphere. In fact, aerosols' greatly enhanced forward scattering causes the lowest inverse CCT's (the purest blues) to occur not at  $\Psi = 90^\circ$ , but instead from  $90^\circ < \Psi < 110^\circ$ , close to the minimum of the aerosol-scattering phase function.

## 4. SPECTRAL ANALYSIS

Spectral analysis of our skylight measurements is also instructive, and we do this with a principal value decomposition of the kind that Parkinen *et al.* describe.<sup>42</sup> Let  $E_E(\lambda)$  be an experimentally determined skylight spectrum. We can reconstruct it approximately by using  $p$  eigenvectors in the equation

$$E_R(\lambda) = \sum_{i=1}^p \langle E_E(\lambda) | V_i(\lambda) \rangle V_i(\lambda), \quad (2)$$

where  $E_R(\lambda)$  is the reconstructed spectrum,  $V_i(\lambda)$  the  $i$ th eigenvector, and  $\langle | \rangle$  denotes the inner product. To test this reconstruction's accuracy, we once again use a goodness of fit coefficient<sup>43–45</sup> (GFC) that is based on the Schwartz's inequality. In our work, this coefficient is

$$\text{GFC} = \frac{\left| \sum_j E_E(\lambda_j) E_R(\lambda_j) \right|}{\left[ \sum_j [E_E(\lambda_j)]^2 \right]^{1/2} \left[ \sum_j [E_R(\lambda_j)]^2 \right]^{1/2}}. \quad (3)$$

In fact, the GFC is the multiple correlation coefficient  $R$ , the square root of  $E_R(\lambda)$ 's spectral variance with respect to the original  $E_E(\lambda)$ . The GFC ranges from 0 to 1, with 1 corresponding to an exact duplicate of  $E_E(\lambda)$ . We found that colorimetrically accurate  $E_R(\lambda)$  require a  $\text{GFC} \geq 0.995$ ; what we call "good" spectral fit requires a  $\text{GFC} \geq 0.999$ , and  $\text{GFC} \geq 0.9999$  is necessary for "excellent" fit.<sup>43,44</sup>

We plot the first five eigenvectors  $V(\lambda)$  for our Granada skylight dataset in Fig. 14, and collectively they account for 99.9% of its measured spectral variance. The second skylight  $V(\lambda)$  corresponds to the dataset's yellow–blue variations, as earlier research has shown.<sup>18,23</sup> Yet in a departure from earlier results, our third skylight  $V(\lambda)$  does not account for the dataset's purple–green variations. Instead this eigenvector produces Granada chromaticity displacements that nearly parallel the CIE daylight locus.

Although we use the CIE method to recover skylight spectra from their corresponding 1931 chromaticities,<sup>36</sup> we update it by using the Granada skylight locus [Eq. (1)] and skylight eigenvectors (Fig. 14). The CIE suggests using just the first three  $V(\lambda)$ , which for our data yields a mean GFC of just 0.9900: Only 53.3% of our  $E_R(\lambda)$  are of "acceptable" quality, while "good" and "excellent"  $E_R(\lambda)$  are limited to only 21.4% and 1.91%, respectively.

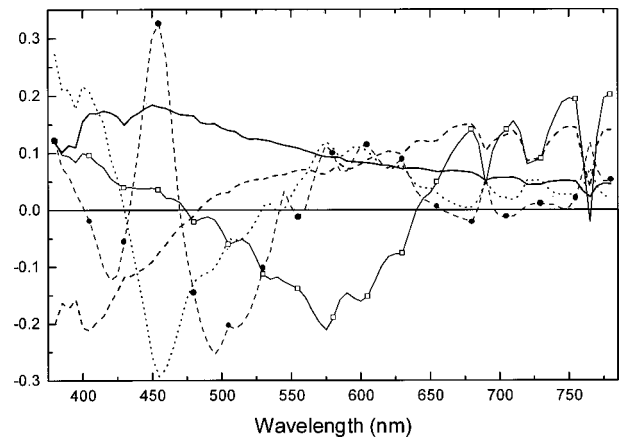


Fig. 14. Spectral distribution of the first five eigenvectors for the Granada skylight basis set from 380–780 nm. Solid curve,  $p = 1$  eigenvector (mean vector); dashed curve,  $p = 2$  eigenvector; dotted curve,  $p = 3$  eigenvector; solid curve with open squares,  $p = 4$  eigenvector; dashed curve with solid circles,  $p = 5$  eigenvector.

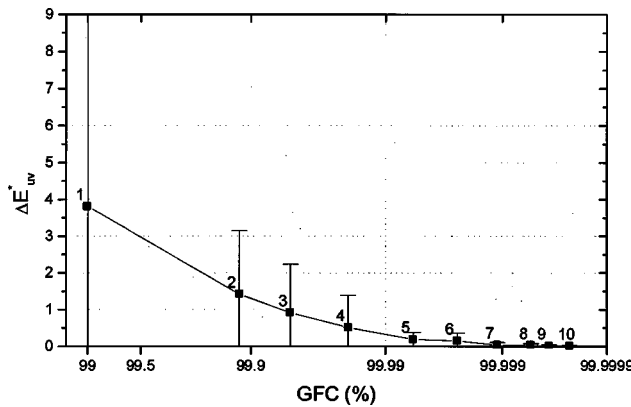


Fig. 15. Mean CIELUV color difference  $\Delta E^*_{uv}$  as a function of mean GFC. Numbers next to each point indicate the number of eigenvectors  $p$  necessary in Eq. (2) to yield the given GFC. Error bars are 2 standard deviations wide.

This limited spectral accuracy arises because the CIE method permits reconstruction of exact  $E_R(\lambda)$  only if we use chromaticities *exactly* on the given locus [Eq. (1), here]. Clearly very few of our measured chromaticities meet this criterion, and this reduces the mean spectral accuracy of our  $E_R(\lambda)$ .

What happens if we step outside the CIE recommendations and test different  $p$  values in Eq. (2)? Now we calculate the resulting GFC values and CIELUV color differences  $\Delta E^*_{uv}$  between the original and reconstructed spectra. As we see in Fig. 15 we must use at least the first three  $V(\lambda)$  in order to get “good” mean quality, whereas “excellent”  $E_R(\lambda)$  require five  $V(\lambda)$ . For more than 95% of our  $E_R(\lambda)$  to be of “acceptable,” “good,” or “excellent” quality, we require 2, 4, or 6  $V(\lambda)$ , respectively. Although in principle metamerism can decouple colorimetric accuracy from spectral accuracy, Fig. 15 indicates that in principal our mean  $\Delta E^*_{uv}$  depends strongly on the average spectral GFC.

Figure 15 also shows the dependence of mean  $\Delta E^*_{uv}$  on the number of  $V(\lambda)$  used. As  $p$  increases, colorimetric errors decrease sharply, especially for the first three eigenvectors. In technical or industrial applications, three or five  $\Delta E^*_{uv}$  units are often taken to be a JND. Figure 15 shows that, by using  $p = 3$  in Eq. (2), we ensure not only a mean  $\Delta E^*_{uv} < 3$  units, but also that its associated standard deviation is  $< 3$  units. Our analysis shows, in agreement with CIE recommendations, that in fact three  $V(\lambda)$  are required to reconstruct a skylight spectrum that is colorimetrically and photometrically indistinguishable from its original  $E_E(\lambda)$ .

## 5. CONCLUSIONS

Among the many new observations stemming from our skylight measurement campaign, several stand out. First, the CIE daylight locus only approximates Granada’s great variety of clear skylight, which has CCTs ranging from 3804 K to  $\infty$  K and inverse CCT peaks at 70–75  $\text{MK}^{-1}$ . Second, our new Granada locus [Eq. (1)] more accurately measures local skylight variability than does the CIE locus. In particular, our locus is farther from the

greens than any other published daylight or skylight loci. This in turn suggests the value of developing different skylight loci for different types of sites rather than relying on just one locus worldwide.

Third, chromaticity curves along the  $\phi_{\text{rel}} = 0^\circ, 90^\circ$  meridians (the principal plane and its perpendicular) form distinct V shapes that nearly coincide with the CIE locus. Fourth, at all relative azimuths we found distinct asymmetries in color and luminance at geometrically equal  $h, \phi_{\text{rel}}$ . These differences usually are suprathreshold, and they can be as large as 4–5 JND or 8% in luminance. Contrary to the simplifying assumptions made in many clear-sky scattering models, such asymmetries are routinely perceptible in the real atmosphere. Fifth, our principal value decomposition shows that three eigenvectors (in agreement with CIE recommendations) are needed to reconstruct colorimetrically accurate skylight spectra. However, six eigenvectors are required for *spectrally* accurate skylight spectra.

Although skylight chromaticities and spectra have been measured precisely for several decades, our work shows that new measurements can still spur valuable new theoretical and practical insights. For example, our quantification of clear-sky color and luminance asymmetries suggests how much variability a truly comprehensive visible-wavelength radiative transfer model must accommodate. As for practical applications, our work easily lets us calculate (1) diffuse sky spectral irradiance on sloping surfaces and (2) skylight chromaticities that are angularly integrated over FOV’s much larger than  $3^\circ$ . Thus anytime or anywhere that skylight rather than daylight proper dominates the daytime sky, our new observations can have great utility.

## ACKNOWLEDGMENTS

J. Hernández-Andrés and J. Romero were supported by Spain’s Comisión Interministerial de Ciencia y Tecnología (CICYT) under research grant PB96-1454. R. L. Lee was supported by United States National Science Foundation grant ATM-9820729 and by the United States Naval Academy’s Departments of Mathematics and Physics.

Javier Hernández-Andrés can be reached by e-mail at javierha@ugr.es.

1. C. F. Bohren and A. B. Fraser, “Colors of the sky,” *Phys. Teach.* **23**, 267–272 (1985).
2. F. C. Hooper, A. P. Brunger, and C. S. Chan, “A clear sky model of diffuse sky radiance,” *J. Sol. Energy Eng.* **109**, 9–14 (1987).
3. R. Perez, J. Michalsky, and R. Seals, “Modelling sky luminance angular distribution for real sky conditions: experimental evaluation of existing algorithms,” *J. Illum. Eng. Soc.* **21**, 84–92 (1992).
4. F. M. F. Siala, M. A. Rosen, and F. C. Hooper, “Models for the directional distribution of the diffuse sky radiance,” *J. Sol. Energy Eng.* **112**, 102–109 (1990).
5. C. R. Prasad, A. K. Inamdar, and H. P. Venkatesh, “Computation of diffuse radiation,” *Sol. Energy* **39**, 521–532 (1987).
6. R. Perez, R. Seals, and J. Michalsky, “All-weather model for sky luminance distribution—preliminary configuration and validation,” *Sol. Energy* **50**, 235–245 (1993).
7. A. W. Harrison and C. A. Coombes, “Angular distribution of

- clear sky short wavelength radiance," *Sol. Energy* **40**, 57–63 (1988).
8. E. M. Winter, T. W. Metcalf, and L. B. Stotts, "Sky-radiance gradient measurements at narrow bands in the visible," *Appl. Opt.* **34**, 3681–3685 (1995).
  9. G. Zibordi and K. J. Voss, "Geometrical and spectral distribution of sky radiance: comparison between simulations and field measurements," *Remote Sens. Environ.* **27**, 343–358 (1989).
  10. C. Chain, D. Dumortier, and M. Fontoynt, "A comprehensive model of luminance, correlated colour temperature and spectral distribution of skylight: comparison with experimental data," *Sol. Energy* **65**, 285–295 (1999).
  11. S. Sekine, "Spectral distributions of clear sky light and their chromaticities," *J. Light Visual Environ.* **15**, 23–32 (1991).
  12. R. L. Lee, Jr., "Colorimetric calibration of a video digitizing system: algorithm and applications," *Color Res. Appl.* **13**, 180–186 (1988).
  13. R. L. Lee, Jr., "Twilight and daytime colors of the clear sky," *Appl. Opt.* **33**, 4629–4638 (1994).
  14. G. Wyszecki and W. S. Stiles, *Color Science: Concepts and Methods, Quantitative Data and Formulae* (Wiley, New York, 1982), p. 11.
  15. S. T. Henderson and D. Hodgkiss, "The spectral energy distribution of daylight," *Br. J. Appl. Phys.* **14**, 125–131 (1963).
  16. G. J. Chamberlin, A. Lawrence, and A. A. Belbin, "Observations on the related colour temperature of north daylight in southern England," *Light Light* **56**, 70–72 (1963).
  17. H. R. Condit and F. Grum, "Spectral energy distribution of daylight," *J. Opt. Soc. Am.* **54**, 937–944 (1964).
  18. D. B. Judd, D. L. MacAdam, and G. Wyszecki, "Spectral distribution of typical daylight as a function of correlated color temperature," *J. Opt. Soc. Am.* **54**, 1031–1041 (1964).
  19. Y. Nayatani and G. Wyszecki, "Color of daylight from north sky," *J. Opt. Soc. Am.* **53**, 626–629 (1963).
  20. J. F. Collins, "The color temperature of daylight," *Br. J. Appl. Phys.* **16**, 527–532 (1965).
  21. G. T. Winch, M. C. Boshoff, C. J. Kok, and A. G. du Toit, "Spectroradiometric and colorimetric characteristics of daylight in the southern hemisphere: Pretoria, South Africa," *J. Opt. Soc. Am.* **56**, 456–464 (1966).
  22. S. R. Das and V. D. P. Sastri, "Spectral distribution and color of tropical daylight," *J. Opt. Soc. Am.* **55**, 319–323 (1965).
  23. V. D. P. Sastri and S. R. Das, "Typical spectral distributions and color for tropical daylight," *J. Opt. Soc. Am.* **58**, 391–398 (1968).
  24. Y. Nayatani, M. Hitani, and H. Minato, "Chromaticity and spectral energy distribution of daylight from north sky at Amagasaki, Japan," *Bull. Electrotech. Lab.* **31**, 1127–1135 (1967).
  25. A. W. S. Tarrant, "The spectral power distribution of daylight," *Trans. Illum. Eng. Soc.* **33**, 75–82 (1968).
  26. G. L. Knestrick and J. A. Curcio, "Measurements of the spectral radiance of the horizon sky," Rep. 6615 (U.S. Naval Research Laboratory, Washington, D.C., 1967).
  27. V. D. P. Sastri and S. B. Manamohanam, "Spectral distribution and colour of north sky at Bombay," *J. Phys. D* **4**, 381–386 (1971).
  28. E. R. Dixon, "Spectral distribution of Australian daylight," *J. Opt. Soc. Am.* **68**, 437–450 (1978).
  29. L. T. Maloney and B. A. Wandell, "Color constancy: a method for recovering surface spectral reflectance," *J. Opt. Soc. Am. A* **3**, 29–33 (1986).
  30. D. H. Marimont and B. A. Wandell, "Linear models of surface and illuminant spectra," *J. Opt. Soc. Am. A* **9**, 1905–1913 (1992).
  31. LI-1800 spectroradiometer from LI-COR, Inc., 4421 Superior St., Lincoln, Neb. 68504-1327.
  32. C. Riordan, D. R. Myers, R. Hulstrom, W. Marion, C. Jennings, and C. Whitaker, "Spectral solar radiation data base at SERI," *Sol. Energy* **20**, 67–79 (1989).
  33. D. R. Myers, "Estimates of uncertainty for measured spectra in the SERI spectral solar radiation database," *Sol. Energy* **43**, 347–353 (1989).
  34. S. Nann and C. Riordan, "Solar spectra irradiance under clear and cloudy skies: measurements and semiempirical model," *J. Appl. Meteorol.* **30**, 447–462 (1991).
  35. S. T. Henderson, *Daylight and Its Spectrum* (American Elsevier, New York, 1970), pp. 173–184.
  36. Ref. 14, pp. 144–146.
  37. J. Hernández-Andrés, R. L. Lee, Jr., and J. Romero, "Calculating correlated color temperatures across the entire gamut of daylight and skylight chromaticities," *Appl. Opt.* **38**, 5703–5709 (1999).
  38. Ref. 14, pp. 224–225.
  39. Ref. 14, pp. 306–310.
  40. R. L. Lee, Jr., "Digital imaging of clear-sky polarization," *Appl. Opt.* **37**, 1465–1476 (1998).
  41. M. P. Thekaekara, "Solar energy outside the earth's atmosphere," *Sol. Energy* **14**, 109–127 (1973).
  42. J. P. S. Parkkinen, J. Hallikainen, and T. Jaaskelainen, "Characteristic spectra of Munsell colors," *J. Opt. Soc. Am. A* **6**, 318–322 (1989).
  43. J. Romero, A. García-Beltrán, and J. Hernández-Andrés, "Linear bases for representation of natural and artificial illuminants," *J. Opt. Soc. Am. A* **14**, 1007–1014 (1997).
  44. J. Hernández-Andrés, J. Romero, A. García-Beltrán, and J. L. Nieves, "Testing linear models on spectral daylight measurements," *Appl. Opt.* **37**, 971–977 (1998).
  45. J. Hernández-Andrés, "Características espectrales y colorimétricas de la luz-día y luz-cielo en Granada," Ph.D. dissertation (Universidad de Granada, Spain, 1999).